SAND99-1944C

Development of characterization tools for reliability testing of MicroElectroMechanical system actuators

Norman F. Smith*, William P. Eaton, Danelle M. Tanner, and James J. Allen

Sandia National Laboratories, P.O. Box 5800, MS 1081, Albuquerque, NM 87185-1081

ABSTRACT

Characterization tools have been developed to study the performance characteristics and reliability of surface micromachined actuators. These tools include 1) the ability to electrically stimulate or stress the actuator, 2) the capability to visually inspect the devices in operation, 3) a method for capturing operational information, and 4) a method to extract performance characteristics from the operational information.

Additionally, a novel test structure has been developed to measure electrostatic forces developed by a comb drive actuator.

Keywords: MicroElectroMechanical Systems, MEMS Actuator Reliability, MEMS Characterization, Performance Tools, Image Analysis

1. INTRODUCTION

The microelectronics industry has long had a large suite of tools for performing characterization, parameter extraction, and reliability testing of integrated circuits. These tools are supplied by a large number of various manufacturers. As MEMS become more commercially feasible, a new set of measurement tools is needed.

MEMS are typically classified into two types, sensors and actuators. The characterization of MEMS sensors can be performed with the same types of tools that are used in the microelectronics industry. These sensors typically output an electrical signal that is easily measured, with the input stimulus coming from a controllable environmental condition. However, the MEMS actuator (e.g. – Sandia fabricated microengine in Figure 1) is much more difficult to characterize since it performs work based on its input stimulus. The work that is performed, ranging from rotating a gear transmission to popping up a mirror[1, 2], is not easily meas-

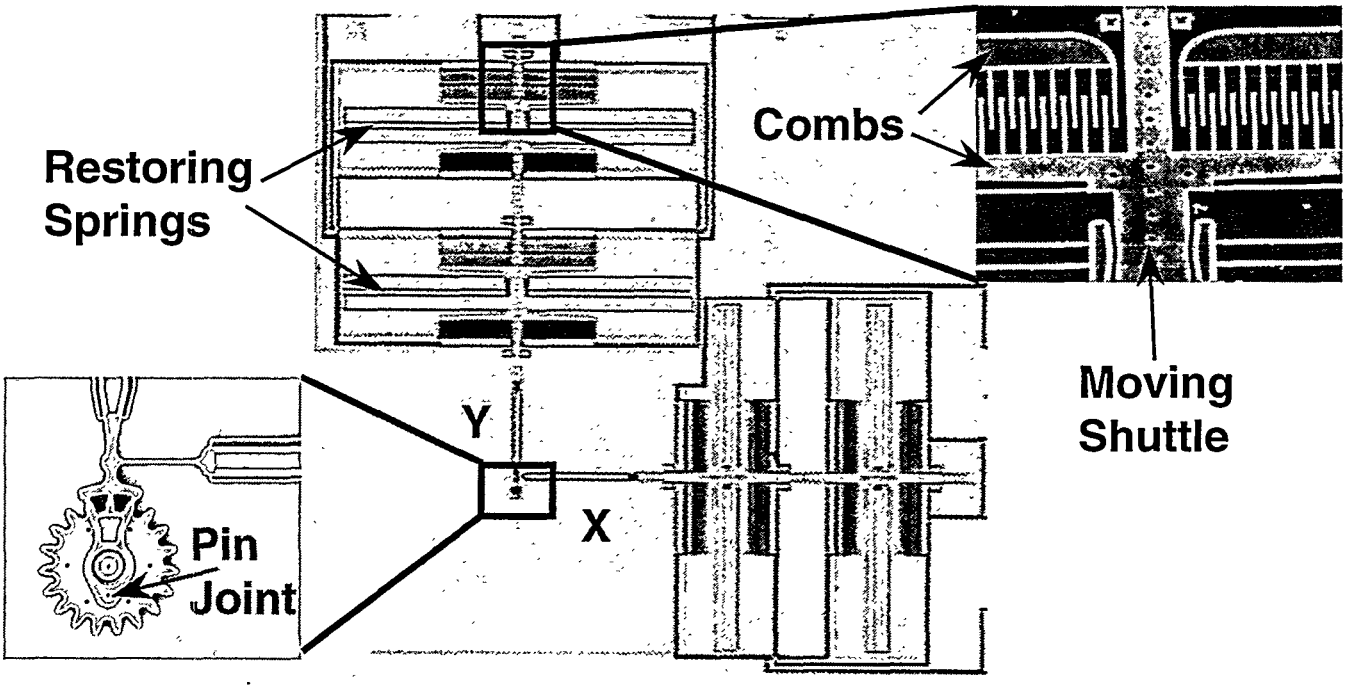

Figure 1. Sandia microengine with expanded views of the comb drive (top right) and the rotating gear (bottom left) shown in what we define at $\theta = 0$.

*Correspondence: Email: smithnf@sandia.gov; WWW: http://www.mdl.sandia.gov/Micromachine

with comparable velocities. The latter are about 1+ for $v<<v_0$. Consequently, SHCI neutralize and de-excite rapidly when they interact with solid surface. Mean charge equilibration times of SHCI like Xe^{44+} and Th^{75+} in thin carbon foils have been found to be only about 7 fs [4]. Loss of kinetic energy of ions to target electrons and nuclei is significantly enhanced during charge equilibration [5-7]. The potential energy of SHCI, i. e., the sum of the binding energies of the electrons removed from the ion, is dissipated during de-excitation. This potential energy, 51 keV and 198 keV for Xe^{44+} and Th^{75+}, is deposited initially in a nanometer scale target volume close to the surface. The equivalent power density in this process is $\sim 10^{14}$ W/cm^2. De-excitation of SHCI already begins above surfaces by the resonant capture of target electrons and the formation of hollow atoms. Except for grazing incident collisions, only a small fraction of the potential energy can be dissipated before ions reach the surface, because the available time is too short at the given rates for Auger and radiative transitions. Hollow atom formation and decay in and above metallic and insulating targets has been investigated in great detail in measurements of secondary electron emission, Auger electron and x-ray spectroscopy [1-3]. Atomic force microscopy has been applied to the characterization of nanometer size defects on mica surfaces [2, 8] and on self assembled monolayers [3, 9] formed by the impact of individual SHCI. Insulators, semiconductors and thin semimetals react to the intense, ultrafast electronic excitation imposed by SHCI with the emission of large numbers of secondary ions and neutrals. A theory of electronic sputtering by SHCI has to describe microscopic mechanisms for the transfer of projectile potential energy, or electronic excitation energy, into kinetic energy of sputtered particles [10]. Defect mediated sputtering by SHCI up to Xe^{27+} was demonstrated for LiF and

DISCLAIMER

SiO_2 [11, 12]. Sputtering by Coulomb explosions [1, 3, 10] was found to be consistent with results for uranium oxide and SHCI like Th^{70+} [13]. A third model considers effects of high densities of electronic excitation on the structural stability of solids. This approach can explain the very large sputter yields found for GaAs under impact of Th^{70+} [14]. In the following, we will discuss some of the experimental challenges in measurements of sputtering yields, before reviewing the results on sputter yield measurements in light of complementary theories.

The finding of secondary ion intensities in the order of 0.1 to 5 secondary ions detected per SHCI [15] stimulated interest in the development of SHCI based surface analysis in a time-of-flight secondary ion mass spectrometry scheme [16-18]. The detection of more than one secondary ion from one impact event with high enough (>0.01) probability allows for the analysis of correlations in secondary ion emission. Since multiple secondary ions are emitted by individual projectiles from an area of only a few tens of nm^2, coincidence analysis can deliver information on chemical structure and composition of materials on a nanometer length scale [17]. We will present results on the characterization of sub-micron copper lines and copper particles on SiO_2 by this approach in chapter IV.

2. Experimental techniques for sputter yield measurements

Two established techniques for the measurement of sputter yields in particle solid interactions are the microbalance and the catcher techniques. The former uses an quartz crystal to monitor the change in resonance frequency associated with the mass change of the irradiated surface as a function exposure time. The sensitivity of this technique has

been extended to allow for measurements of mass changes as low as 1E-3 monolayers [1]. While this sensitivity is impressive, application of the microbalance technique for measurement of sputter yields in the order of 10 atoms removed per projectile requires a beam current of a few nA or about 1E10 projectiles per second. Beam currents of this order are routinely extracted from ECR sources but only for ions with charge states below about 30+ for xenon.

In the catcher or collector technique, sputtered particles are collected on a secondary target for *in situ* or *ex situ* analysis after accumulation of a sufficiently high surface coverage [10, 19]. Recently, Mieskes et al, have reported on *in situ* analysis of catcher targets in studies of sputtering yields of metals by high energy heavy ions (~1 MeV/u) [20]. Using a 1.5 MeV carbon beam they were able to detect Ti on Si at coverages in the low 1E13 atoms/cm^2 range.

For the sputter yield measurements with SHCI from the EBIT at Lawrence Livermore National Laboratory, collectors consisted of thin (50 to 150 nm) SiO_2 layers on silicon substrates. In order to maximize the collection efficiency, catcher targets were placed at a distance of 6 mm from the sputter targets, resulting in a view factor of 0.1. Beams of SHCI at 0.3 v_0 impinged on GaAs and UO_2 targets with an incident angle of 30°. Targets were cleaned in situ and surface conditions were monitored by secondary ion mass spectrometry with highly charged projectiles (HCI-SIMS) [3, 12, 13]. Beam intensities for extraction of SHCI from an EBIT are in the order of 1E6 Xe^{44+}/s and 1E5 Au^{69+}/s . At a sputtering yield of 10 atoms per projectile, surface coverages of sputtered materials after exposures of several days are only in the order of 1E11 atoms/cm^2. These low coverages provided excellent samples for sensitivity tests of HCI-SIMS [18].

Quantitative analysis of catcher targets was performed at the heavy ion backscatter facility at Sandia National Laboratory [21] using beams of 100 KeV carbon ions. The sensitivity of HIBS for detection of heavy elements on otherwise clean silicon is in the order of 1E9 atoms/cm^2. In figure 1 we show an example of HIBS analysis of a catcher target (150 nm SiO_2 on Si) with a uranium coverage of 3.3 (+/-0.3) E11 atoms/cm^2.

Relative uncertainties in sputter yields determined with the collector technique are stem from uncertainties in HIBS results, dose uncertainties, and variations in the view factors between measurements and range typically from +/-10-30%. One contribution to the systematic error stems from assumptions on sticking probabilities of secondary particles on the catcher surface. Typical values for the latter are >0.9 [22]. Another uncertainty lies in the assumption of a cosine angular distribution of secondary particles in the calculation of the view factor. Analysis of catcher targets is a standard technique for determination of actual angular distributions of secondary neutrals [19]. This approach requires a distance between target and collector that is large compared to the spot size of the primary beam. The increased target-collector distance corresponds to a reduction in the achievable surface coverage. With the current beam intensity limitations for SHCI such a reduction of surface coverage was prohibitive. Overall systematic uncertainties for sputtering yield values determined for SHCI from EBIT with the catcher technique are about +/-50%.

Secondary ion yields from GaAs and UO_2 samples were measured by time-of-flight secondary ion mass spectrometry with SHCI as projectiles [15-18]. Briefly, SHCI are extracted from EBIT and impinge on samples under normal incidence for analysis in a low resolution, high transmission instrument. Samples are biased to a few thousand volts

positive or negative bias and secondary ions are accelerated to an extraction grid and then drift to an annular microchannelplate detector. The detection efficiency of this arrangement is ~0.15. Time-of-flight cycles are started by secondary electrons or protons that are emitted following the impact of individual projectiles. This single ion triggering scheme allows for a timing resolutions of 1 ns and an efficiency of practically 100% in negative polarity and >80% in positive polarity for SHCI like Xe^{44+}. Conventional TOF-SIMS instruments use electronic starts derived from the pulsing of a compressed ion pulse and can achieve the nanosecond timing resolution needed for competitive mass resolution [23]. This approach is impractical for SHCI at the currently available beam intensities. For catcher analysis, secondary ions were extracted into a reflectron type time-of-flight spectrometer with a mass resolution, $m/\Delta m$, of about 1000 at m=28 u [18].

3. Sputter yields: Results and discussion

Results from sputter yield measurements for CsI [10], LiF [11, 12], SiO_2 [12], GaAs [12, 14, 24] and UO_2 [13] are shown in Fig. 2 as a function of potential energy of SHCI [3].

The model of defect mediated desorption can explain sputter yields of several hundred target atoms per projectile with the formation and successive decay of electronic defects such as self trapped excitons and self trapped holes in alkali halides and SiO_2 [11, 12]. The study by Weathers et al. also showed how efficient electronic excitation energy is transferred to kinetic energy of sputtered particles in materials were such electronic defects can form [10]. Here, yields were dominated by electronic energy loss of 60 KeV

Ar ions and the increase as a function of projectile charge from q=4+ to q=11+ was small on the background of this offset.

Results for GaAs are most controversial. The absence of yield increases for very slow Ar^{q+} up to 8+ is consistent with the defect mediated sputtering model since the latter can not be formed in GaAs [12]. On the contrary, the finding of increasing ablation rates for Ar^{q+} up to 9+ was interpreted in terms of a phenomenological Coulomb explosion model by Mochiji et al. [24]. Results from experiments with highly charged xenon and thorium ions showed a dramatic increase of sputtering yields to a value of 1410 +/-210 atoms/Th^{70+} [14]. Measurements of secondary ion yields allowed for a determination of the ionization probabilities of secondary ions, and, contrary to expectations from a simple Coulomb explosion model, the ionization probability was found to decrease for very high charge states. The high sputtering yields for GaAs can be understood when considering the structural stability of covalent solids under condition of intense, ultrafast electronic excitation induced by de-exciting SHCI [3, 14]. This approach was developed for the description of femtosecond melting of Si and GaAs where high densities (>1E22 cm^{-3}) of electronic excitations were induced by femto second lasers [25].

For UO_2, total yields were also found to increase as a function of potential energy of SHCI, but secondary ion yields were found to increase stronger, resulting in an increase of the ionization probability of positive secondary ions by about an order of magnitude to a value of 5-7% [13]. Also, spectra of positive secondary ions showed series of uranium oxide clusters, which could be detected up to $(UO_2)_7^+$. Relatively high ionization probabilities and significant cluster ion emission are consistent with a coulomb explosion

model. However, contributions from defect formation and effects of high excitation densities could also contribute.

Very high secondary ion yields and cluster ion emission has also been observed for SiO_2 targets [15, 16]. For this material all three of the above processes are likely to contribute to sputtering by SHCI [26]. Detailed experimental and theoretical [27] studies are necessary to differentiate contributions from competing mechanisms as a function of excitation intensity.

4. Applications of HCI-SIMS

The potential of SHCI like Xe^{44+} for applications in surface analysis lies in the fact that these ions produce up to three orders of magnitude more secondary ions than singly charged projectiles [9, 13-15].

In HCI-SIMS, each time-of-flight cycle is started by the impact of an individual projectile. Time-of flight secondary ion mass spectrometry (TOF-SIMS) spectra can be taken both in histogram mode or in list mode. In the former, TOF-cycles from consecutive projectiles are simply summed up to form a spectrum. Typically, accumulation of cycles from impact of a few million projectiles yields sufficient statistics and accumulation times are about 10 min. In list mode, time-of-flight cycles (i. e., the start trigger and associated stops from secondary ions) from each projectile are stored separately. Then, conditions on the presence of selected mass peaks are selected when TOF-cycles are summed up. The resulting coincidence spectra show correlations between selected secondary ions or molecular ions that were detected. Each projectile forms secondary ions from a surface area with an estimated size of only a few tens of

nanometers, and the correlations therefore contain considerable information about local composition. The probability for the detection of n secondary ions following the impact of a one Xe^{44+} projectile is shown in Fig. 3. Targets were a bulk copper sample with a native oxide layer and a test wafer with 800 nm wide copper interconnect lines imbedded in a 25 nm TaO diffusion barrier layer in SiO_2 [28]. HCI-SIMS data were taken with the reflectron type analyzer and were accumulated for 5E6 projectiles. At the given transmission of the reflectron, the probability for detection of two secondary ions is about 10%. Up to eleven secondary ions have been detected from one individual sputtering event. Detection of more than one secondary ion with such high probability makes the analysis of correlation effects between secondary ions practical.

The correlation coefficient, C(A, B), gives a measure for the probability to detect a secondary ion B in coincidence with ion A [17, 29, 30]:

$$C(A,\ B) = \frac{P(A,B)}{P(A)\ P(B)}$$

Here, P(A) and P(B) are the probabilities for the detection of secondary ions A and B independently in all impact events. P(A, B) is the probability for detection of A and B in the same impact event. For C(A, B) >1, it is more likely to detect A when B is also present. An example of correlation coefficients is given in Fig. 4 a) for secondary ions from the copper interconnect sample. The probability to detect a $^{65}Cu^+$ is increased when $^{63}Cu^+$ was also detected in the impact event. $^{65}Cu^+$ and $^{63}Cu^+$ are both emitted when a highly charged ions probes an area on one of the copper lines. On the contrary, C(A, B) <1 indicates an anti-correlation between, e. g. emission of $^{28}Si^+$ and $^{65}Cu^+$ or $^{63}Cu_2^+$. Here, it is very unlikely to detect both a copper and a silicon ion from the same impact event. This anti-correlation is characteristic for well separated structures of different

chemical composition. Statistical uncertainties in values of correlation coefficients are typically smaller than +/-20% (not shown).

Detection of TaO^+ ions from the Ta barrier layer is, at the given level of statistical uncertainly, weakly anti-correlated to both silicon and copper ions. This is expected for a well separated, intact barrier layer and also demonstrates that highly charged ions do indeed probe surface features on a length scale of a few tens of nm.

In contrast, copper ions emitted from the bulk copper sample show no significant correlations (Fig 4b).

In another example of coincidence analysis the sample was a SiO_2 wafer which had been coated with a solution of $CuSO_4$. The surface coverage of the copper oxide was about 0.03 monolayers. Fig. 5 shows correlation coefficients with very strong correlations between copper and copper oxide molecular ions. These correlations indicating the presence of well separated copper oxide and silicon dioxide areas on the surface and would not be expected for a blanket deposit of evenly separated copper oxide molecules. The latter is energetically unfavorable and the formation of islands has been studied extensively in the context of the early stages of thin film growth. Fig. 6 shows a section of an HCI-SIMS spectrum with positive secondary ions emitted from the $CuSO_4/SiO_2$ sample. The detection of copper oxide clusters is consistent with the presence of copper oxide islands or particles on the surface. Comparison of our results with results from direct imaging techniques [31] is subject of ongoing studies.

5. Summary

Electronic sputtering in the interaction of slow, highly charged ions with insulators and semiconductors .....

Acknowledgements

The authors gratefully acknowledge the excellent technical support at the LLNL EBIT facility provided by D. Nelson and E. Magee. This work was performed under the auspices of the U. S. Department of Energy by Lawrence Livermore National Laboratory under contract No. W-7405-ENG-48. Part of this work was supported by NIST.

References:

[1] A. Arnau, F. Aumayr, P. M. Echenique, M. Grether, W. Heiland, J. Limburg, R. Morgenstern, P. Roncin, S. Schipers, R. Schuch, N. Stolterfoht, P. VArga, T. J. M. Zouros, and H. Winter, Surf. Sci. Rep. 27 (1997) 113

[2] D. H. G. Schneider, M. A. Briere, Phys. Scr. 53 (1996) 228

[3] T. Schenkel, A. V. Hamza, A. V. Barnes, and D. H. Schneider, Prog. Surf. Sci., in press

[4] M. Hattass, T. Schenkel, A. V. Hamza, A. V. Barnes, M. W. Newman, J. W. McDonald, T. R. Niedermayr, G. A. Machicoane, and D. H. Schneider, Phys. Rev. Lett. 82, 4795 (1999)

[5] T. Schenkel, M. A. Briere, A. V. Barnes, A. V. Hamza, K. Bethge, H. Schmidt-Böcking, and D. Schneider, Physical Review Letters **79,** 2030 (1997); T. Schenkel, A. V. Hamza, A. V. Barnes, and D. H. Schneider, Physical Review A **56** R1701 (1997)

[6] J. I. Juaristi, A. Arnau, P. M. Echenique, C. Auth and H. Winter, Phys. Rev. Lett. **82,** 1048 (1999)

[7] M. A. Briere, T. Schenkel, D. H. Schneider, P. Bauer, A. Arnau, Phys. Scr. **T73,** 324 (1997)

[8] D. C. Parks, M. P. Stockli, E. W. Bell, L. P. Ratkliff, R. W. Schmieder, F. G. Serpa, and J. P. Gillaspy, Nucl. Instrum. Meth. Phys. Res. B **134,** 46 (1998)

[9] T. Schenkel, M. Schneider, M. Hattass, M. W. Newman, A. V. Barnes, A. V. Hamza, and D. H. Schneider, J. Vac. Sci. Technol. B **16,** 3298 (1998).

[10] D. L. Weathers, T. A. Tombrello, M. H. Prior, R. G. Stokstad, R. E. Tribble, Nuclear Instruments and Methods in Physics Research B **42,** 307 (1989)

[11] T. Neidhart, F. Pichler, F. Aumayr, HP. Winter, M. Schmid and P. Varga, Physical Review Letters **74**, 5280 (1995); Nuclear Instruments and Methods in Physics Research B **98,** 465 (1996)

[12] M. Sporn, G, Libiseller, T. Neidhart, M. Schmid, F. Aumayr, HP. Winter, and P. Varga, Physical Review Letters 79, 945 (1997); P. Varga, T. Neidhard, M. Sporn, G. Libiseller, M. Schmid, F. Aumayr and HP. Winter, Phys. Scr. **T73**, 307 (1997)

[13] T. Schenkel, A. V. Barnes, A. V. Hamza, J. C. Banks, B. L. Doyle, D. H. Schneider, Physical Review Letters **80**, 4325 (1998)

[14] T. Schenkel, A. V. Barnes, A. V. Hamza, J. C. Banks, B. L. Doyle, D. H. Schneider, Physical Review Letters **81**, 2590 (1998)

[15] T. Schenkel, A. V. Barnes, M. A. Briere, A. V. Hamza, A. Schach von Wittenau, D, H. Schneider, Nuclear Instruments and Methods in Physics Research B **125,** 153 (1997); T. Schenkel et al., Materials Science Forum **248-249,** 413 (1997); T. Schenkel et al., Phys. Rev. Lett. **78**, 2481 (1997)

[16] T. Schenkel, A. V. Hamza, A. V. Barnes, D. H. Schneider, D. S. Walsh, and B. L. Doyle, Journal of Vacuum Science and Technology A **16** (1998) 1384.

[17] A. V. Hamza, T. Schenkel, A. V. Barnes, and D. H. Schneider, Journal of Vacuum Science and Technology A **17**, 303 (1999).

[18] T. Schenkel, A. V. Hamza, A. V. Barnes, M. W. Newman, G. Machicoane, T. Niedermayr, M. Hattass, J. W. McDonald, K. J. Wu, R. W. Odom, and D. H.

Schneider, Proceedings of the IX International Conference on the Physics of Highly Charged Ions, Bensheim, Physica Scripta, T80, 1999, in press.

[19] H. H. Andersen and H. L. Bay, in Sputtering by Particle Bombardment I, R. Behrisch (ed.) (Springer, Berlin, 1981), P. 145-218

[20] H. D. Mieske, W. Assmann, M. Brodale, M. Dobler, H. Glückler, P. Hartung, and P. Stenzel, Nucl. Instrum. Meth. Phys. Res. B **146**, 162 (1998)

[21] J.C. Banks, B. L. Doyle, J. A. Knapp, D. Werho, R. B. Gregory, M. Anthony, T. Q. Hurd, and A. C. Diebold, Nucl. Instr. Methods Phys. Res. B **138**, 1223 (1998); J. A Knapp, J. C. Banks, and B. L. Doyle, Nuclear Instruments and Methods in Physics Research B **85**, 20 (1994).

[22] K. G. Liebrecht, J. E. Griffith, R. A. Weller, and T. A. Tombrello, Radiat. Eff. **49**, 195 (1980)

[23] A. Benninghoven, Angew. Chem. Int. Ed. Engl. **33**, 1023 (1994)

[24] K. Mochiji, N. Itabashi, S. Yamamoto, H. Shimizu, S. Ohtani, Y. Kato, H. Tanuma, K. Okuno, N. Kobayashi, Surf. Sci. **357-358**, 673 (1996); Jpn. J. Appl. Phys. **34**, 6861 (1995)

[25] P. Stampfli, Nuclear Instruments and Methods in Physics Research B **107**, 138 (1996); P. Stampfli, K. H. Bennemann, Applied Physics A **60**, 191 (1996)

[26] H. Gnaser, *Low-Energy Ion irradiation of Solid Surfaces* (Springer, Berlin, 1999)

[27] H. P. Cheng, and J. D. Gillaspy, Phys. Rev. B **55**, 2628 (1997)

[28] H. Li, D. J. Hymes, J. de Larios, I. A. Mowat, and P. M. Lindley, Micro, March 1999, P. 35

[29 T. Schenkel, K. J. Wu, H. Li, M. W. Newman, A. V. Barnes, J. W. McDonald, and A. V. Hamza, Proceedings of the 1st International Conference on Advanced Materials and Processes for Microelectronics, San Jose, March 1999, to be published

[30] E. F. da Silveira, S. B. Duarte and E. A. Schweikert, Surf. Sci. **408**, 28 (1998)

[31] A. C. Diebold, P. Lindley, J. Viteralli, J. Kingsley, B. Y. H. Liu, and K.-S. Woo, J. Vac. Sci. Technol. A **16**, 1825 (1998)

Figure captions:

Figure 1.: Heavy ion backscattering spectrum from of a U-SiO_2 (150 nm on Si) catcher target (solid) and an unexposed witness target (dashed). Projectiles were carbon at 120 keV. The incident charge was 10 μC. The uranium coverage was 3.3 (+/-0.3) E11 atoms/cm^2.

Figure 2: Total sputtering yields for CsI, solid squares, [10]; LiF, open circles, [11, 12]; SiO_2, solid triangles, [12]; GaAs, solid circles, [12], open diamonds [24], solid diamonds [14]; and UO_2 [13] vs. potential energy of projectile. Kinetic energies of projectiles were constant within each data set but varied in measurements by different groups.

Figure 3: Probability, P(n) for the detection of n secondary ions following the impact of one Xe^{44+} ion on a SiO_2 sample with 800 nm wide Cu interconnects.

Figure 4: a) Correlation coefficients from coincidence analysis of secondary ions from a Cu-interconnect sample and b) from a bulk copper target.

Figure 5: Correlation coefficients from coincidence analysis of a $CuSO_4/SiO_2$ sample with a copper oxide coverage of 0.03 monolayers.

Figure 6: TOF-SIMS spectrum from the $CuSO_4/SiO_2$ sample with copper oxide and SiO_2 cluster ions. Projectiles were Xe^{48+} with a kinetic energy of 557 keV.

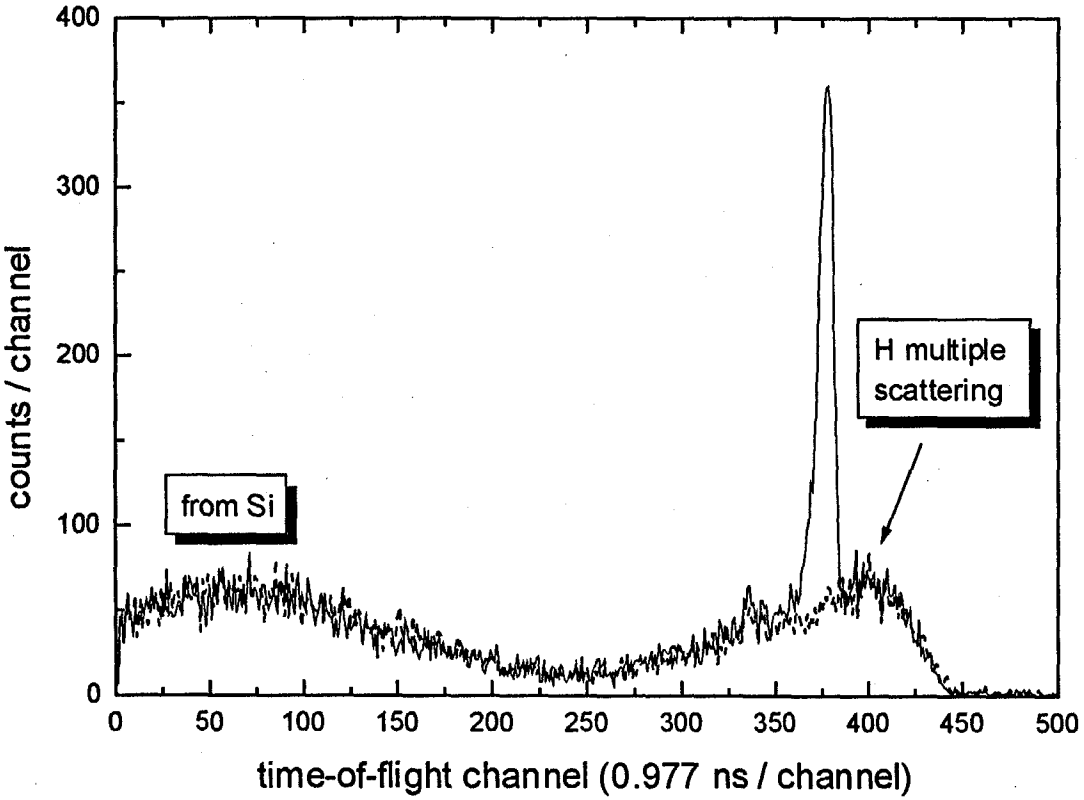
400
300
200
100
0
counts / channel
from Si
H multiple
scattering
0
50
100
150
200
250
300
350
400
450
500
time-of-flight channel (0.977 ns / channel)

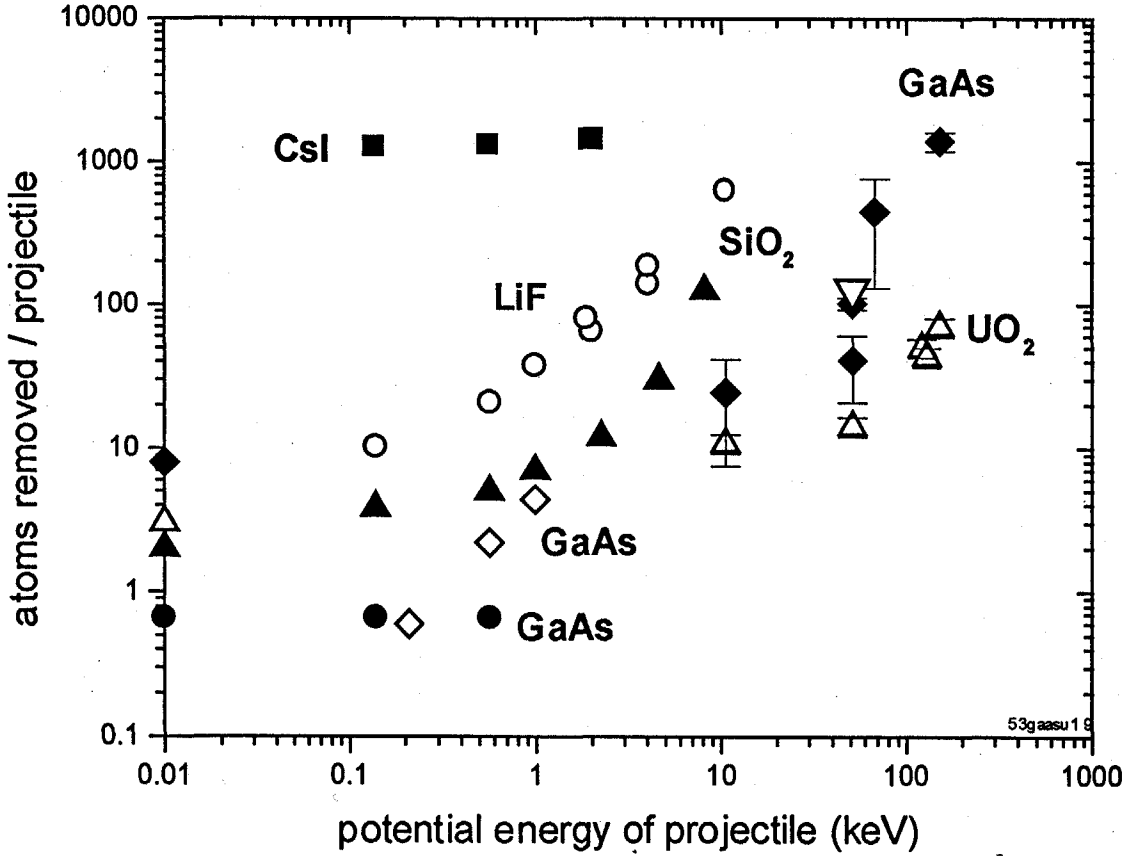
10000
1000
100
10
1
0.1
0.01
0.1
1
10
100
1000
atoms removed / projectile
potential energy of projectile (keV)
CsI
LiF
SiO2
GaAs
UO2
GaAs
GaAs
53gaasu1 9

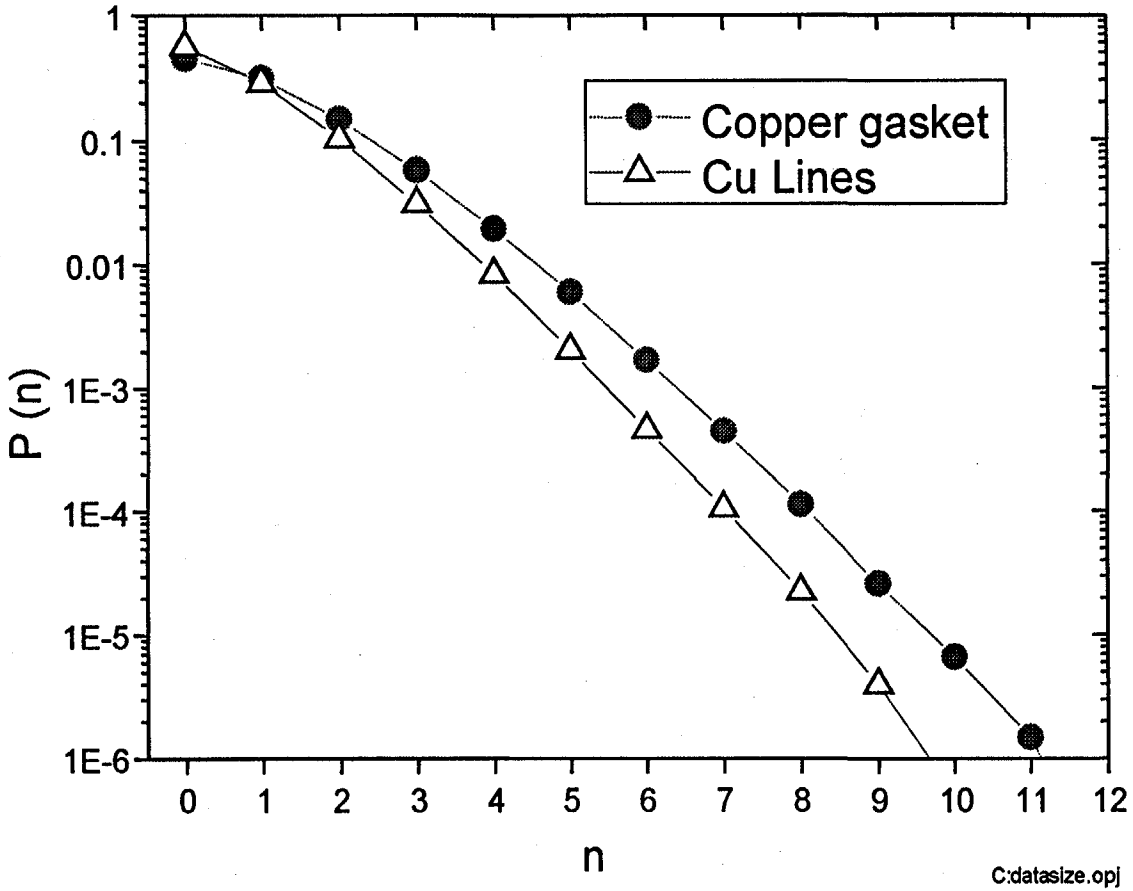
Copper gasket
Cu Lines
P (n)
n
1
0.1
0.01
1E-3
1E-4
1E-5
1E-6
0
1
2
3
4
5
6
7
8
9
10
11
12
C:datasize.opj

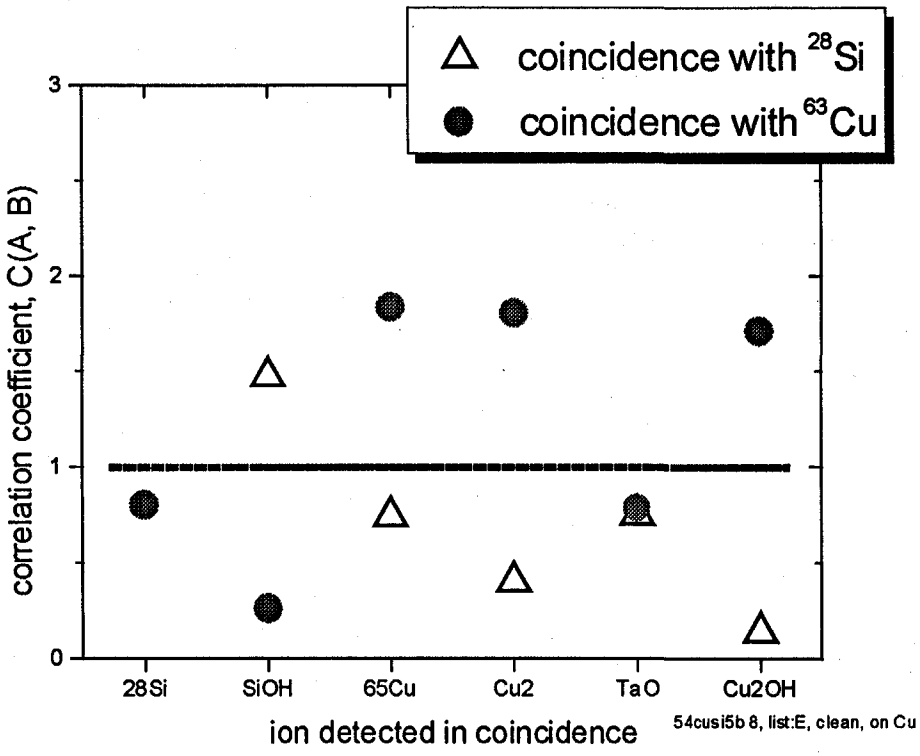
coincidence with ^{28}Si
coincidence with ^{63}Cu
correlation coefficient, C(A, B)
3
2
1
0
28Si
SiOH
65Cu
Cu2
TaO
Cu2OH
ion detected in coincidence
54cusi5b 8, list:E, clean, on Cu

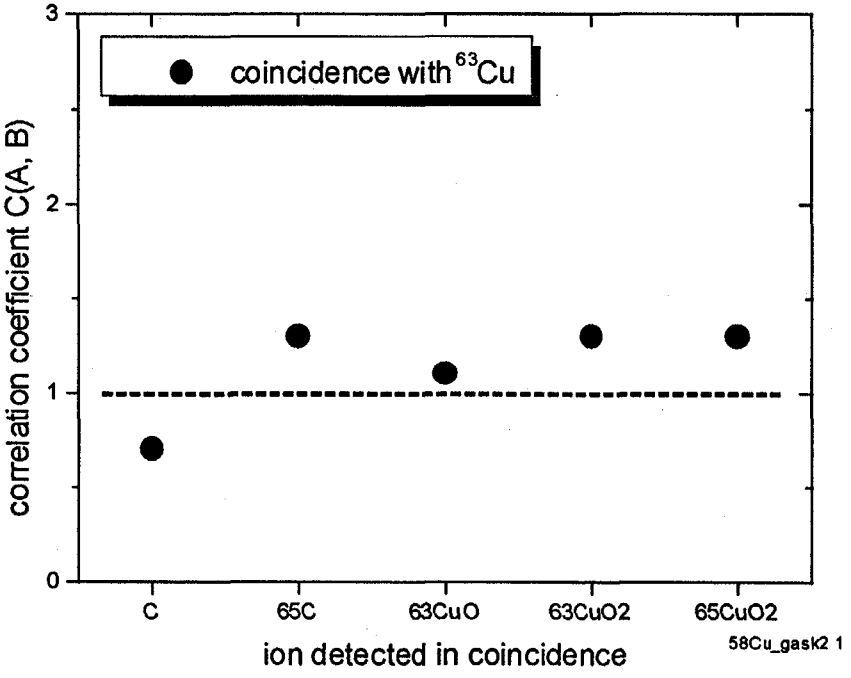
coincidence with ^{63}Cu
correlation coefficient C(A, B)
3
2
1
0
C
65C
63CuO
63CuO2
65CuO2
ion detected in coincidence
58Cu_gask2 1

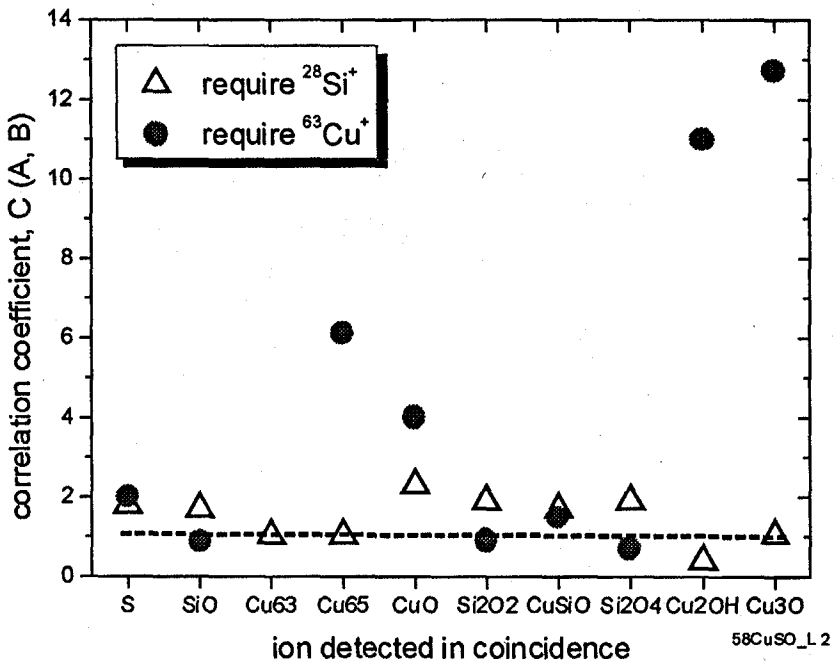
require $^{28}Si^{+}$
require $^{63}Cu^{+}$
correlation coefficient, C (A, B)
0
2
4
6
8
10
12
14
S
SiO
Cu63
Cu65
CuO
Si2O2
CuSiO
Si2O4
Cu2OH
Cu3O
ion detected in coincidence
58CuSO_L 2

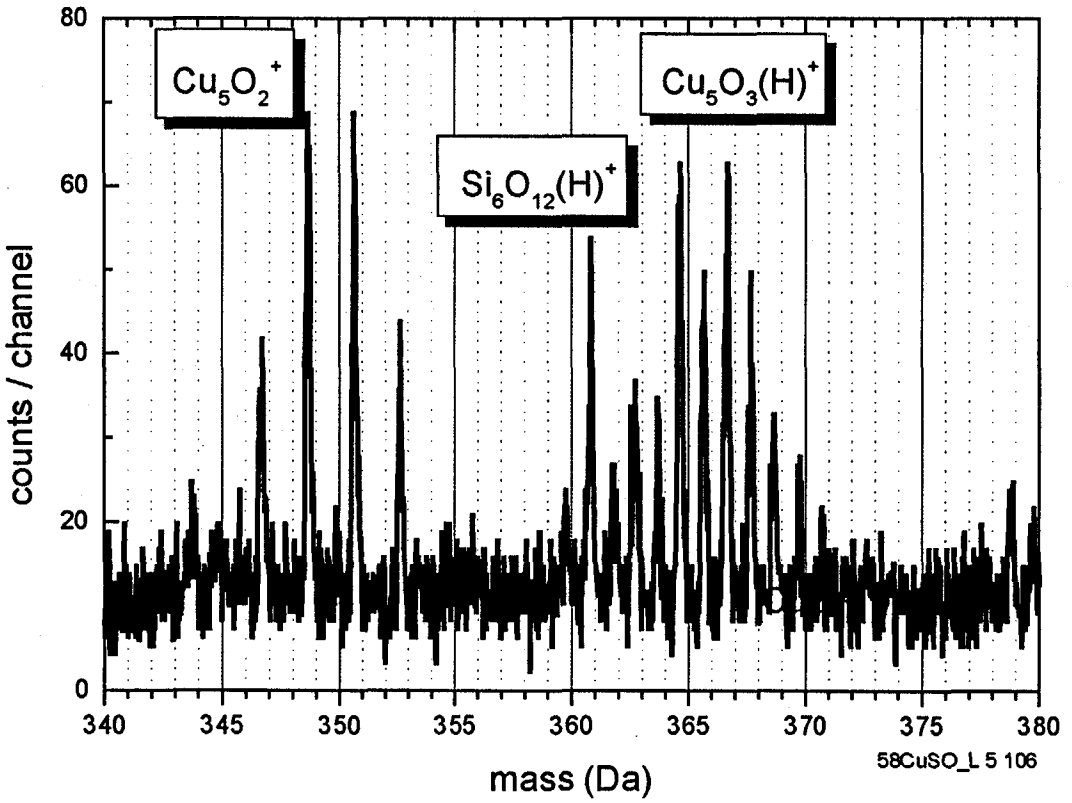
80
60
40
20
0
counts / channel
340
345
350
355
360
365
370
375
380
mass (Da)
$Cu_5O_2^+$
$Si_6O_{12}(H)^+$
$Cu_5O_3(H)^+$
58CuSO_L 5 106